Domain decomposition of level set updates for salt segmentation

Taylor Dahlke, Biondo Biondi and Robert Clapp

SUMMARY

Level set methods can provide a sharp interpretation of the salt body by defining the boundary as an isocontour of a higher dimensional implicit surface. We can use shape optimization to derive a gradient update that evolves the implicit surface to minimize the Full-Waveform Inversion (FWI) objective function. We can decompose the update gradient into separate partitions with individual scaling parameters to better avoid local minima, and more effectively converge on the true model. Using our approach on synthetic examples, we can achieve reasonable convergence of the residual L2 norm, as well as the evolution of the velocity toward the true model, demonstrating the feasibility of this approach. Ultimately, this method could be integrated into processing work-flows to improve the building and refining of the velocity models used for imaging.

INTRODUCTION

Some previous approaches to performing salt body segmentation use a shape optimization approach for identifying salt body boundaries (Guo and de Hoop (2013); Lewis et al. (2012)), by applying a global step parameter to the update gradient. However, the back-propagation of the residuals can create boundary updates that lead to a local minima when applied this way. We show how decomposing the update gradient can help avoid this problem. I will discuss the general derivation, the fundamental problem that we address, the algorithm we apply, and the results we obtain.

The boundaries of a salt body can be represented as the zero isocontour of a higher dimensional surface ϕ (for example, a 2D boundary as a contour of a 3D surface). A gradient can be derived to evolve the surface ϕ according to the FWI objective function:

$$F(m) \doteq \frac{1}{2}\|A(m)-d\|_2^2. \quad (1)$$

Unlike the smooth boundaries produced by tomographic approaches, the isocontour resulting from the shape optimization provides a sharp boundary, which is a more appropriate way to classify most salt-sediment interfaces.

Derivation of the evolution equation

While it may seem counter-intuitive to add an extra dimension to our problem, by doing so, we gain the advantage of easily merging/separating bodies as the evolution proceeds, as well as the ability to handle sharp corners and cusps in the lower-dimensional (2D) plane on which the boundary exists.

Osher and Sethian (1988) and Burger (2003) describe the level set of ϕ that represents the salt body boundary as:

$$\phi(x_\Gamma, \tau) = 0.$$

By taking the derivative of this equation, applying the chain rule, and re-arranging terms we can get:

$$\frac{\partial \phi}{\partial \tau} = -V(x_\Gamma, \tau)\,|\nabla \phi|\,. \quad (2)$$

The scalar speed term $V(x_\Gamma, \tau)$ describes the magnitude of the variation of ϕ that is normal to the boundary Γ. It determines the evolution of the implicit surface, and ultimately the boundary implied by it. We derive this normal velocity such that the FWI objective function is minimized.

Calculus of variations

The shape derivative we use is based on a formal calculus of variations outlined in Santosa (1996). The objective is to define the variation of the model m with respect to the boundary variation (represented implicitly by the surface, ϕ).

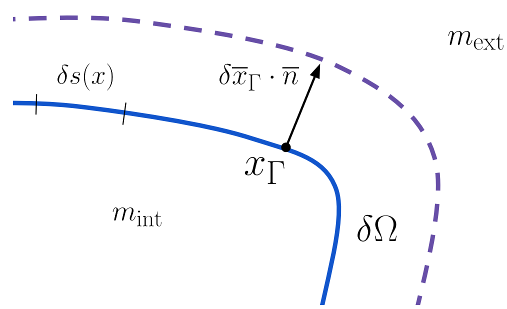

Figure 1: The geometry of the curve $\{x_\Gamma : \phi = 0\}$ for a variation $\delta\phi(x)$ for an evolution step τ.

We begin by considering an inner product of δm with a test function $f(x)$. Formally, this can be written as,

$$\langle \delta m, f(x) \rangle = \int_{R^2} \delta m(x) f(x) dx = \int_{\partial\Omega} \delta m(x) f(x) dx. \quad (3)$$

Because the $\delta m(x)$ term equals zero in $R^2 \setminus \partial\Omega$, it does not contribute to the overall inner product when integrating over that domain; therefore, we only integrate over $\partial\Omega$ where $\delta m(x)$ is non-zero. We know that $\delta m(x)$ will be $\pm(m_{int} - m_{ext})$, depending on the relative values of m_{int} and m_{ext} or the direction of the normal vector $\vec{n}$. We only care about the component of δx_Γ that occurs in the normal direction, because a tangential variation of x_Γ does not affect m or ϕ. Furthermore, because δx_Γ is infinitesimal, we can replace dx with $\vec{\delta x_\Gamma} \cdot \vec{n}$ and simplify Equation 3 into

DOI http://dx.doi.org/10.1190/segam2015-5917368.1

$$\langle \delta m, f(x)\rangle = \int_{\partial\Omega}(m_{int} - m_{ext})\vec{\delta x_\Gamma}\cdot\vec{n} f(x) ds(x), \tag{4}$$

where $ds(x)$ is the incremental arc length along the boundary Γ. We can think of $\vec{\delta x_\Gamma}\cdot\vec{n}ds(x)$ as roughly the incremental area over which m varies at x.

We can identify δm from Equation 4. It can be considered a measure over $\partial\Omega$:

$$\delta m = (m_{int} - m_{ext})\vec{\delta x_\Gamma}\cdot\vec{n}\,|_{x\in\partial\Omega}\,. \tag{5}$$

We remember that in the previous section we stated the goal of this derivation as being a solution of the scalar velocity function $V(x_\Gamma, \tau)$, such that the objective function is minimized. We recognize that the normal component of the variation δx_Γ satisfies:

$$\vec{\delta x_\Gamma}\cdot\vec{n} = V(x_\Gamma, \tau). \tag{6}$$

We can use the shape derivative formulation described in Santosa (1996) to find a $V(x_\Gamma, \tau)$ that minimizes the FWI objective function (Equation 1) that we insert into Equation 2 to get a final implicit surface update gradient of:

$$\frac{\partial\phi}{\partial\tau} = (m_{int} - m_{ext})\frac{\partial F}{\partial m}\left|\vec{\nabla}\phi\right|. \tag{7}$$

The adjoint state method as described in Plessix (2006) is used to derive $\frac{\partial F}{\partial m}$, which can be shown to be equivalent to $F(m)^T(A(m) - d)$. Because our case uses the FWI objective function (Equation 1), this term can be interpreted as least squares migration, more specifically as reverse time migration (RTM). This result is formulated as:

$$\frac{\partial F(m)}{\partial m} = -\sum_s \int_0^T \int_{x\in\Gamma} h_s(x,t)\frac{\partial^2 u_s(x,t)}{\partial t^2} d\sigma dt. \tag{8}$$

This term by itself is the velocity model perturbation, which we can process and use to make tomographic updates as described in the following section.

APPLICATION

Our algorithm is demonstrated on 2D velocity models, with the implicit surface evolved being a 3D surface. For the forward wave propagation, a wavelet with a 15.0 Hertz (Hz) central frequency and 4 millisecond (ms) time sampling was propagated using a time domain forward operator.

General evolution algorithm

We begin with an initial background velocity, and a binary valued (-1, 1) function as the initial implicit surface ϕ. We create a full initial-guess velocity model (m_o) assuming a constant salt velocity. Using m_o, we forward model to get our d_{syn} and subsequently find our residual. From the residual we calculate both a tomographic and a boundary update gradient. Because the RTM image is based on a non-smoothed model, it contains reflection and tomography information. We get our tomography update by smoothing the RTM image to mitigate reflection updates that are present. We then perform a non-linear line search for α in a manner that minimizes the FWI objective function; and then, apply an explicit forward Euler scheme that updates the background velocity V_{back}. Following this step, we perform the same line search and update steps for the implicit surface (ϕ):

$$\phi^{j+1} = \phi^j + (\beta\frac{\partial\phi}{\partial j} + \mu G_{reg}) \tag{9}$$

$$V^{j+1}_{back} = V^j_{back} + \alpha\frac{\partial V_{back}}{\partial j}. \tag{10}$$

where β and α are the step sizes, and j is the current iteration point. G_{reg} is a distance-regularization term that maintains the slope of the implicit surface, such that $|\nabla\phi| = 0$. By driving the gradient of the implicit surface to equal one, we minimize irregularities of the implicit surface during evolution. This regularization term is calculated according to the approach described in Li et al. (2010). The full work flow is graphically represented in Figure 2.

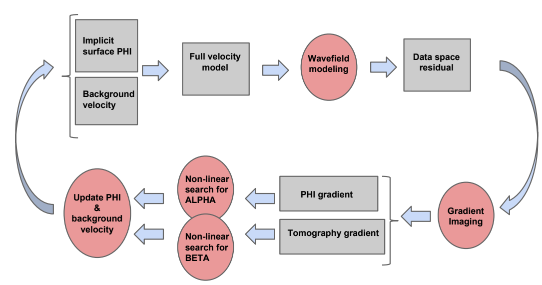

Figure 2: The general work flow used for shape optimization.

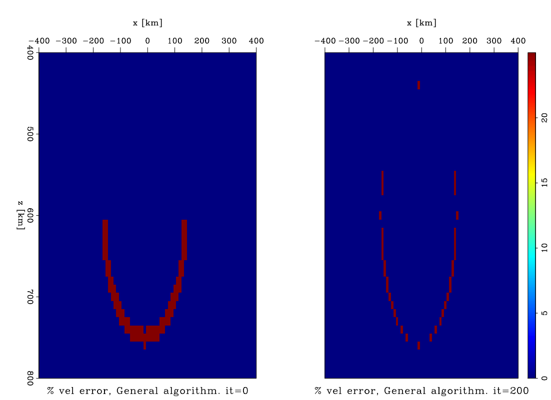

Figure 3: Velocity model error for starting model (left), and final model (right) after 200 iterations using general algorithm.

DOI http://dx.doi.org/10.1190/segam2015-5917368.1

Boundary update gradient domain decomposition

One notices in Figure 3 that the convergence of the general algorithm just described appears to stall before convergence of the base of salt occurs, even after a significant number of iterations. We hypothesize that the top of salt reflection is dominating the line search for β. To test this, we analyze the gradients derived from a model with perfect top-of-salt (TOS) and background velocity model. Ideally, the gradients should have no update for the TOS, because it is already correct. However, Figure 4 shows that we still realize an update for the TOS.

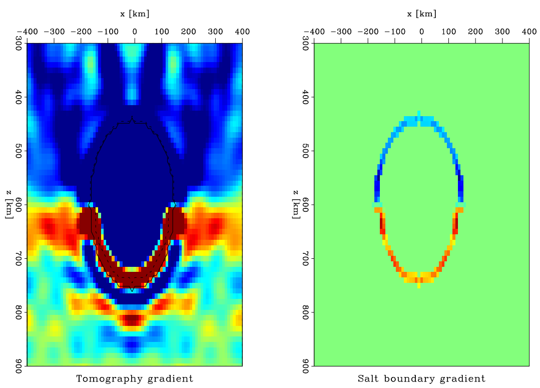

Figure 4: RTM gradient update (left) and ϕ update (right) for model with perfect TOS and background velocity (as shown in the left panel of Figure 3). Blue, decrease; red, increase in velocity (left). Blue, inward boundary movement; red, outward boundary movement (right).

The fundamental problem demonstrated in Figure 4 is that the RTM gradient contains information from both reflector position error, as well as background velocity error. These errors can be difficult or impossible to separate. In this case, the data residual could be correctly removed by changing the position of the bottom reflector, or by making a velocity change above it. The RTM calculation always produces a gradient that applies both these effects; and therefore, we get an incorrect update when illumination for a reflector (like the BOS) is sourced from ray paths that must first travel through another reflector edge of the same body being updated (like the TOS). Because the first reflector event (the TOS) is a stronger event, it converges first and ultimately dominates the line search. The lack of BOS updating caused by this has been observed in recent work (Guo and de Hoop (2013)), and is an inherent problem with the global gradient update approach. Figure 3 shows that even after a significant number of iterations, this approach cannot converge to the true model, and in fact, even becomes worse for some sections of the boundary.

Partitioning approach

A method to de-couple the updating of the TOS and BOS is necessary so that the BOS can continue to be updated even when the TOS converges.

To decompose the ϕ update gradient into "top" and "bottom" components for the general case, we take a dot product of the straight rays from each shot and the boundary-normal vector

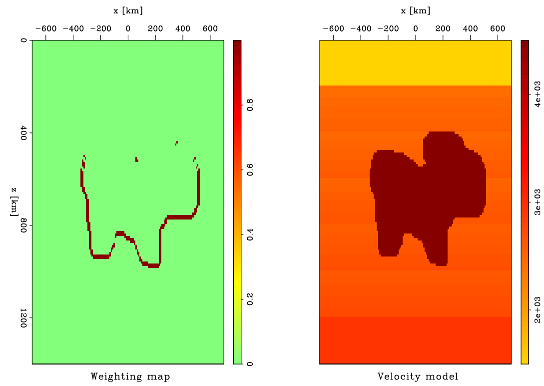

Figure 5: Example of weighting used for the BOS gradient partition (left), and velocity model that weighting is based on (right).

fields, thereby generating a map that approximates the straight ray illumination of the body. We perform these steps for each shot, and sum the dot-product fields. Next, we set all positive values to 1.0 and all negative values to 0.0 (for the TOS weighting map; opposite case for the BOS). Figure 5 gives an example of what this boundary partitioning looks like. This "splitting" has the advantage of decomposing the boundary into sections that generally face away from or toward the acquisition line. Further partitioning of the boundary update can be done by setting thresholding to selectively partition the facing, steep, and shadowed reflecting edges.

Examples

We perform an experiment in which the algorithm does no tomography updating and begins with a perfect background velocity model. Figure 6 shows the results from both the general and decomposed-domain algorithms, demonstrating that the difference between the two approaches is clear. After 50 iterations, the partitioning algorithm has converged on the true model, while the global gradient approach has trouble, particularly on the base of salt.

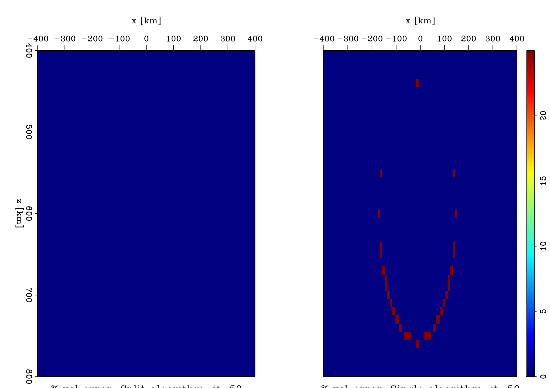

Figure 6: % velocity error at 50 iterations using domain decomposition algorithm (left) and general algorithm (right). Perfect background velocity model.

DOI http://dx.doi.org/10.1190/segam2015-5917368.1

Our next test uses the same salt model with a perturbed background velocity model that we perform tomography updates on. Figure 7 shows that when we apply the decomposed domain approach, we get close convergence with the true model on both the top and base of salt.

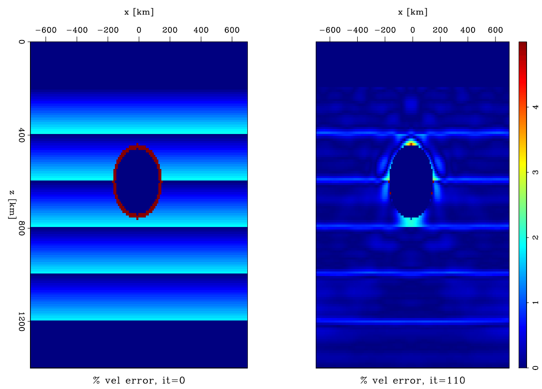

Figure 7: Initial model perturbation (left), and after 110 iterations (right) using split ϕ algorithm.

We compare the decomposed-domain approach results shown in Figure 7 with those from an identical experiment using the general algorithm by plotting the differential error, as shown in Figure 8. From this comparison, we observe that the convergence on the salt model is significantly improved, especially for the base of salt and salt flanks. This further demonstrates that the domain decomposition approach can yield more accurate convergence, even when tomography is also concurrently being updated.

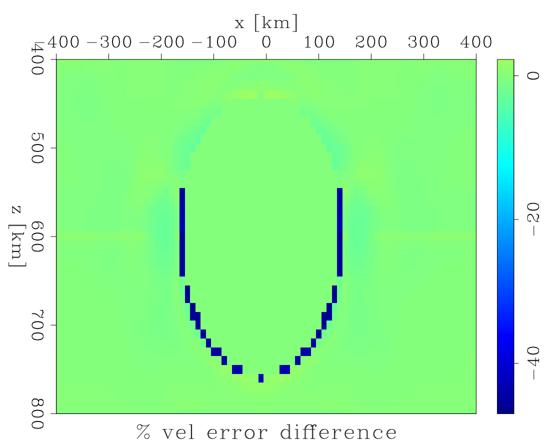

Figure 8: The differential error between the gradient partitioning approach and the general algorithms after 110 iterations, as expressed as a percentage error from the true model. Blue regions are where the domain partitioning approach performs better; red, more poorly.

Figures 9 and 10 show more complex models with generally improved results, with the main exception being the very base of salt in Figure 9. We believe this is caused by the same fundamental problem described previously, because the ray paths illuminating the bottom enter/exit multiple reflectors, and are much weaker events overall, thereby exasperating the problem of coupling this reflector with stronger reflector updates. By partitioning into three domains (top, flanks, and bottom), we may be able to resolve this problem.

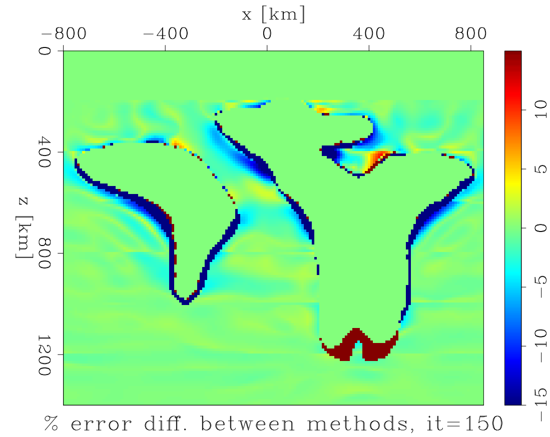

Figure 9: Velocity model difference between general and split ϕ methods, shown as a percentage error from the true model. Blue regions are where the domain partitioning approach performs better; red, more poorly.

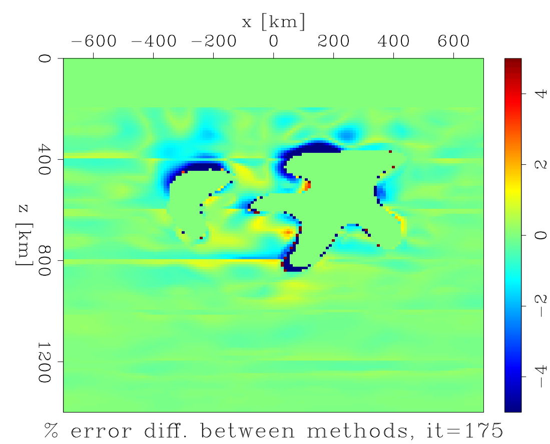

Figure 10: Velocity model difference between general and split ϕ methods, shown as a percentage error from the true model. Blue regions are where the domain partitioning approach performs better; red, more poorly.

Conclusions

Our examples (Figures 8, 9 and 10) show that we get generally better convergence on the base and flanks of salt with the domain decomposition approach. While the very bottom of the salt in Figure 9 has done poorly, we believe that further partitioning of the model (into top, sides, bottom) could allow for better updating on this region. A simple two part split may be insufficient since there are multiple entry/exit points on the ray paths that illuminate this lowest region of the body, which exasperates the problem of coupling this reflector with other reflector updates.

DOI http://dx.doi.org/10.1190/segam2015-5917368.1

REFERENCES

Burger, M., 2003, A framework for the construction of level set methods for shape optimization and reconstruction: Interfaces and Free boundaries, **5**, 301–330.

Guo, Z. and M. de Hoop, 2013, Shape optimization and level set method in full waveform inversion with 3d body reconstruction: SEG Technical Program Expanded Abstracts, 1079–1083.

Lewis, W., B. Starr, D. Vigh, et al., 2012, A level set approach to salt geometry inversion in full-waveform inversion: Presented at the 2012 SEG Annual Meeting.

Li, C., C. Xu, C. Gui, and M. Fox, 2010, Distance regularized level set evolution and its application to image segmentation: Image Processing, IEEE Transactions on, **19**, 3243–3254.

Osher, S. and J. A. Sethian, 1988, Fronts propagating with curvature-dependent speed: algorithms based on hamilton-jacobi formulations: Journal of computational physics, **79**, 12–49.

Plessix, R.-E., 2006, A review of the adjoint-state method for computing the gradient of a functional with geophysical applications: Geophysical Journal International, **167**, 495–503.

Santosa, F., 1996, A level-set approach for inverse problems involving obstacles: ESAIM Controle Optim. Calc. Var, **1**, 17–33.

DOI http://dx.doi.org/10.1190/segam2015-5917368.1

EDITED REFERENCES

Note: This reference list is a copyedited version of the reference list submitted by the author. Reference lists for the 2015 SEG Technical Program Expanded Abstracts have been copyedited so that references provided with the online metadata for each paper will achieve a high degree of linking to cited sources that appear on the Web.

REFERENCES

Burger, M., 2003, A framework for the construction of level set methods for shape optimization and reconstruction: Interfaces and Free Boundaries, 5, 301–330.

Guo, Z., and M. de Hoop, 2013, Shape optimization and level set method in full waveform inversion with 3d body reconstruction: 83rd Annual International Meeting, SEG, Expanded Abstracts, **1**079–1083. http://dx.doi.org/10.1190/segam2013-1057.1.

Lewis, W., B. Starr, and D. Vigh, 2012, A level set approach to salt geometry inversion in full-waveform inversion: 82nd Annual International Meeting, SEG, Expanded Abstracts. http://dx.doi.org/10.1190/segam2012-0737.1.

Li, C., C. Xu, C. Gui, and M. Fox, 2010, Distance regularized level set evolution and its application to image segmentation: IEEE Transactions on Image Processing, **19**, 3243–3254.

Osher, S., and J. A. Sethian, 1988, Fronts propagating with curvature-dependent speed: algorithms based on Hamilton-Jacobi formulations: Journal of Computational Physics, **79**, no. 1, 12–49. http://dx.doi.org/10.1016/0021-9991(88)90002-2.

Plessix, R.-E., 2006, A review of the adjoint-state method for computing the gradient of a functional with geophysical applications: Geophysical Journal International, **167**, no. 2, 495–503. http://dx.doi.org/10.1111/j.1365-246X.2006.02978.x.

Santosa, F., 1996, A level-set approach for inverse problems involving obstacles: ESAIM Controle Optim. Calc. Var, **1**, 17–33. http://dx.doi.org/10.1051/cocv:1996101.

DOI http://dx.doi.org/10.1190/segam2015-5917368.1